ACS OMEGA

http://pubs.acs.org/journal/acsodf

Article

Study of Corrosion Kinetic Measurement and Morphology Observation of Superheater Tube 12Cr1MoV Alloy in Simulated MSWI Flue Gas Containing Varied HCl or SO_2 Concentrations

Xiaobo Liu, Yin Duan, Qian Chen, Ling Long, Guojun Lv, Qunxing Huang, and Xuguang Jiang*

Cite This: *ACS Omega* 2022, 7, 23929−23938

Read Online

ACCESS | Metrics & More | Article Recommendations

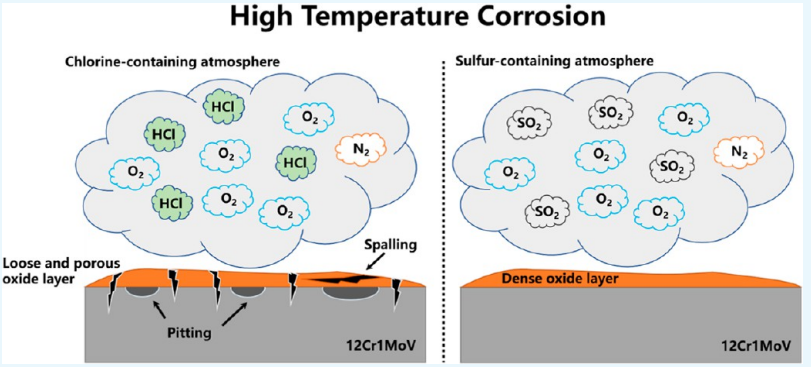

ABSTRACT: Severe corrosion to superheater tubes at high temperatures was gained virtually by gaseous corrosion media, such as HCl and SO_2, in the municipal solid waste incineration flue gas. To clarify the effect of varying concentrations of HCl and SO_2 in the oxidizing atmosphere on the corrosion of 12Cr1MoV, a commercial alloy used in superheaters, two series of corrosion tests under simulated flue gas were performed. Both the corrosion kinetics and corrosion morphology were measured in this work. The results of the present study demonstrated that the addition of HCl was more corrosive than that of SO_2 under an oxidizing atmosphere. The increased HCl concentration had an accelerating effect on the corrosion rate, but the relation between the two was not linear. In contrast, SO_2 exhibited a negligible or even inhibitory effect on corrosion. Both series of test results consistently proved that the temperature had a significant influence on the corrosion of 12Cr1MoV alloy, in particular at 580 °C.

1. INTRODUCTION

Waste to energy (WTE) is playing a pivotal role in the sustainable management of municipal solid waste (MSW).[1] This approach can reduce the demand for landfills and also result in negative CO_2 emissions.[2] In China, the production of MSW is increasing with the rapid economic maturation and large-scale urbanization.[3] The Chinese MSW output grew to 235.12 million tons by 2020, and approximately 60% of MSW was incinerated.[4] Thus, WTE is expected to provide an important strategy for the safe disposal of MSW in China.[3] However, harsh environments generated during MSW combustion, which is characterized by a combination of high levels of NaCl together with HCl and low amounts of SO_2,[5−7] frequently lead to severe corrosion of superheater tubes in WTE boilers.[8] As a consequence, the maintenance costs of WTE plants increase, and the maximum achievable steam temperature of the MSW incineration boilers is limited.[7]

Numerous investigations have examined the corrosive effect of HCl or Cl_2(g) on different superheater materials.[9−15] The corrosive action of gaseous Cl species has been understood to be a specific phenomenon, commonly explained by the "active oxidation" mechanism. In this theory, Cl_2 derived from the oxidation reaction of HCl diffuses through pores and cracks of the oxide scale to the scale−metal interface; thus, metal chlorides are formed.[11,16] These volatile metal chlorides decompose into nonprotective loose metal oxides and Cl_2, when evaporating outward to the scale surface. Then, the regenerated Cl_2 migrates either to the bulk gas or penetrates the oxide scale again to continue a further attack.[17] However, the penetration of chlorine is not fully elucidated in this mechanism.[11]

SO_2 is a species mostly causing sulfidation and enhancing corrosion of heating surfaces in coal, biomass-fired or WTE

Received: May 2, 2022
Accepted: June 17, 2022
Published: June 25, 2022

https://doi.org/10.1021/acsomega.2c02722
ACS Omega 2022, 7, 23929−23938

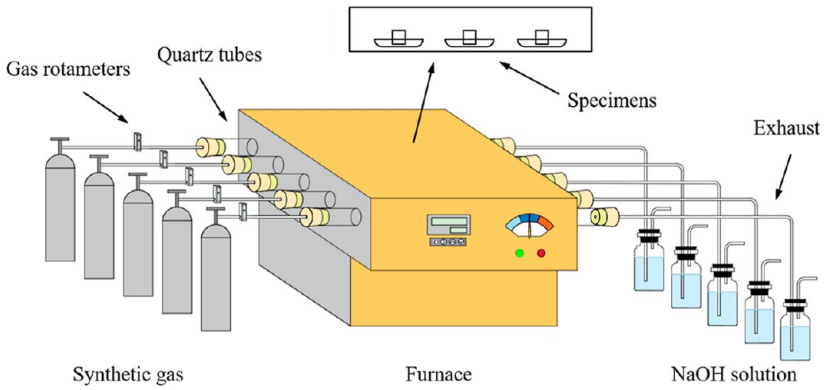

Figure 1. Schematic diagram of the test equipment.

boilers.[11,18−20] In WTE boilers, it is also considered as an intermediate in chlorine corrosion by reacting with alkali metal chlorides to generate Cl_2.[21] Metal corrosion in pure SO_2 or an oxidizing atmosphere containing high concentrations of SO_2 has been studied extensively over the last decades.[22−26] In earlier studies, a higher corrosion rate was usually observed in gases containing SO_2 than that in O_2, which was attributed to the formation of sulfide phases on the scale/metal interface.[18,27,28] However, the effect of SO_2 is still ambiguous. SO_2 has also been reported to inhibit the oxidation of pure Fe if it is present in trace amounts.[29−31]

In the flue gas of the MSW incinerators, the oxygen content is approximately 5−10%,[10,32] and the HCl content is 300−900 ppm,[33−35] while SO_2 is relatively low (3.5−200 ppm).[34,36] Previous work regarding the gas phase corrosion mostly focused on corrosion at a certain high HCl or SO_2 concentration[6,12,37] or a certain temperature.[9,38−40] However, the SO_2 concentration levels were almost low in the Chinese up-to-date operating the WTE plant, and the impact of changes in certain HCl or low SO_2 concentration levels under MSW incineration environments on superheater metal corrosion was poorly understood. Therefore, the objectives of this work are to conduct a comprehensive experiment to investigate the influence of certain HCl concentrations and rather low SO_2 concentrations on high-temperature corrosion of superheater metals in oxidizing atmospheres. The test concentrations of HCl or SO_2 were based on the flue gas environment typically operated in WTE plants in China. The investigated alloy, 12Cr1MoV, is high-strength low-alloy steel with an excellent corrosion resistance and mechanical properties, widely used in superheater tubes at temperatures below 600 °C in biomass boilers and coal-fired boilers.[41] It is also an economical material commonly used in some high superheater and all low superheater tubes in WTE plants in China. In this work, 12Cr1MoV alloy was chosen as the corrosion object to reveal the role of HCl and SO_2 played in MSW flue gas corrosion. In addition, the four temperatures of the superheater tube were chosen to be close to the actual engineering situation according to different steam parameters in the Chinese national standard for WTE plants. Usually, a steam temperature of 400 °C corresponds to a tube temperature of 425−450 °C.[42] In this study, considering the safety margin and simple estimation, we decided to add 60 °C to the steam temperature as the tube wall temperature. Therefore, 460, 510, 545, and 580 °C are the corresponding tube wall temperatures for WTE boilers with steam temperatures of 400, 450, 485, and 520 °C, respectively.

2. MATERIALS AND METHODS

2.1. Material Preparation. A low-alloy steel 12Cr1MoV (nominal composition in wt.%; 1.2Cr-0.35Mo-0.7Mn-0.37Si-0.3V-0.15C-Fe Bal.) was employed in this study. Specimens with a dimension of 10 × 10 × 5 mm were prepared. Before tests, all alloy specimens were ground with SiC grinding paper: 320, 600, and 1000 grit to achieve flat and smooth surfaces. Afterward, the specimens were degreased and cleaned in acetone by ultrasonic agitation. Then, the specimens were dried by a blower, and their dimensions and initial masses were measured and recorded. The dimensions were measured by a vernier caliper with an accuracy of 0.02 mm, including the information of length, width, and height, which were used to calculate the total surface area of each specimen. The masses were measured by a Sartorius electronic balance with an accuracy of 0.0001 g.

2.2. Test Equipment and Process Conditions. The corrosion exposure tests were carried out in a horizontal tube furnace containing five quartz tubes. The furnace was manufactured by Hangzhou LanTian Instrument Co., Ltd, and its model was LT-5-5-10. The maximum heating temperature of the furnace could reach 1000 °C, and the fluctuation degree was only ±1 °C. As illustrated in Figure 1, five quartz tubes can be simultaneously heated to the same temperature, and each quartz tube was equipped with a gas input device and an exhaust gas absorption device. During the test, 12Cr1MoV alloy specimens were placed in each quartz tube in sequence, and atmospheres of different compositions were introduced into each quartz tube for research. Synthetic gas was used in this study to simplify the test equipment. The composition of the synthetic gas was 7% O_2 + 0/300/600/900/1200 ppm HCl + balanced N_2, or 7% O_2 + 0/50/100/150/200 ppm SO_2 + balanced N_2.

In this study, the tests were organized into two series (Table 1). In the first series, the effects of different concentrations of HCl on the high-temperature oxidation of 12Cr1MoV were measured; in the second series, the effects of different low concentrations of SO_2 on corrosion were measured. Five kinds of corrosive atmospheres for each temperature and four temperatures in each series were tested, that is, 20 groups of tests were done in each series. To ensure the consistency of the internal control of each series, the 0%-HCl/SO_2 (pure oxidation) tests as control groups were conducted in both series. In practice, these tests were performed in groups based on different temperatures. For instance, at 460 °C, corrosion tests under oxidizing atmospheres containing 0/300/600/900/1200 ppm HCl can be carried out simultaneously, and

https://doi.org/10.1021/acsomega.2c02722
ACS Omega 2022, 7, 23929−23938

Table 1. High-Temperature Corrosion Test Conditions of 12Cr1MoV Alloy

series	conditions	temperature (°C)
1	0 HCl + 7 vol % O_2 + Bal. N_2	460/510/545/580
	300 ppm HCl + 7 vol % O_2 + Bal. N_2	
	600 ppm HCl + 7 vol % O_2 + Bal. N_2	
	900 ppm HCl + 7 vol % O_2 + Bal. N_2	
	1200 ppm HCl + 7 vol %O_2 + Bal. N_2	
2	0 SO_2 + 7 vol % O_2 + Bal. N_2	460/510/545/580
	50 ppm SO_2 + 7 vol % O_2 + Bal. N_2	
	100 ppm SO_2 + 7 vol % O_2 + Bal. N_2	
	150 ppm SO_2 + 7 vol % O_2 + Bal. N_2	
	200 ppm SO_2 + 7 vol % O_2 + Bal. N_2	

meanwhile, the different kinds of mixed gas were, respectively, injected into five quartz tubes, and other conditions remained the same. 460/510/545/580 °C were chosen for the different superheater tube temperatures for different superheater steam parameters 400/450/485/520 °C accordingly. The exhaust gas was absorbed by passing through a 1 mol/L NaOH solution.

2.3. Test Procedure. The prepared specimens were placed in quartz boats (before the tests, all quartz boats were weighed) since the corrosion products on the surface of the specimens were easy to spall during the corrosion exposure. Then, they were put together into the furnace, which was preheated to a stable temperature. Until the specimens were properly placed in the quartz tubes and the outlets were closed, the tubes were vented with N_2 to prevent the specimens from being preoxidized by the air in the tubes. After that, the corresponding corrosive gas entered each quartz tube separately, with a flow rate of 25 mL/min controlled by a gas rotameter [model LZB-3WB(F)]. The selection of the flow rate referred to previous literatures.[13,43,44] During the exposure, the specimens were placed in the heated zone of the furnace, that is, the middle of the quartz tube, where the temperature fluctuations did not exceed 1 °C. To ensure the test reproducibility, we used three parallel specimens for each test. Tests were conducted for 168 h, and after 24, 72, and 168 h, the specimens were removed out and weighed in their respective boats together with any corrosion products spalled from the specimens. Therefore, the weight change of each specimen after exposure for some time can be calculated according to eq 1

$$\frac{\Delta m}{A} = \frac{m_2 - m_1}{A} \tag{1}$$

where $\Delta m/A$ = the mass gain per unit surface area of the specimen, which is the average of the three parallel specimens, m_1 = the initial mass of the specimen before exposure, and m_2 = the mass of the specimen after exposure for some time.

In the analysis of the SO_2 series test results, the parabolic rate constant was used, the value of which is determined by eq 2

$$\left(\frac{\Delta m}{A}\right)^2 = k_p \cdot t \tag{2}$$

2.4. Material Characterization. To explore the effect of corrosion on metal surfaces, we characterized all corroded specimens using a field emission scanning electron microscope (SEM, S-3700N, Hitachi) at 10 keV of acceleration voltage. The ISO 8407-2021 standard was considered for the corrosion product removal, that is, 12Cr1MoV specimens were dipped in a solution (20−25 °C) containing 50% hydrochloric acid and 0.35% hexamethylene tetramine for 10 min. Preliminary tests have shown that this procedure did not result in the removal of any base metal. To further understand the corrosion mechanism, we also selected the corrosion products under the conditions of 600 ppm HCl and 100 ppm SO_2 for microscopic observation at a high magnification, using an SEM

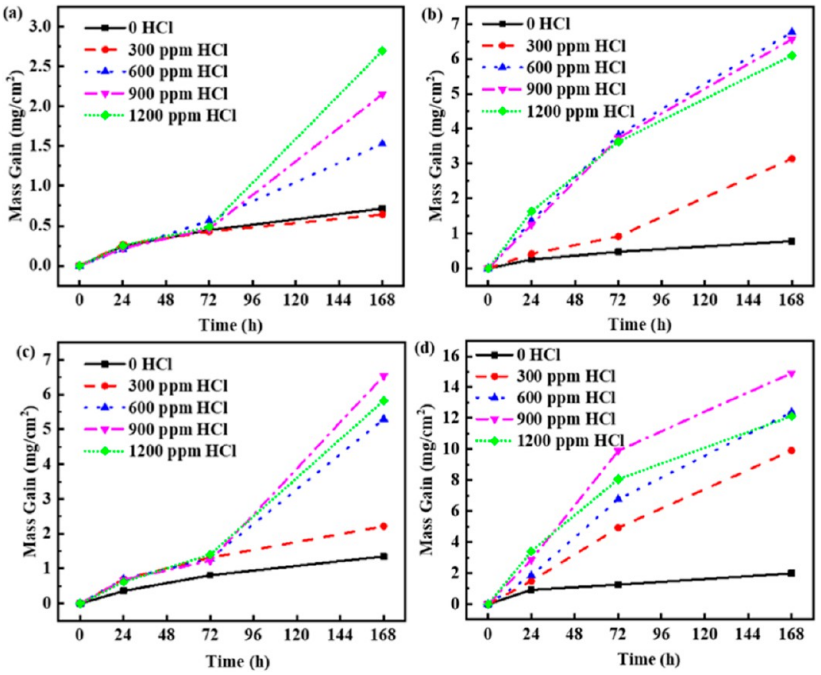

Figure 2. Mass gain of 12Cr1MoV alloy exposed to oxidizing atmosphere containing different concentrations of HCl at (a) 460, (b) 510, (c) 545, and (d) 580 °C for 168 h.

https://doi.org/10.1021/acsomega.2c02722
ACS Omega 2022, 7, 23929−23938

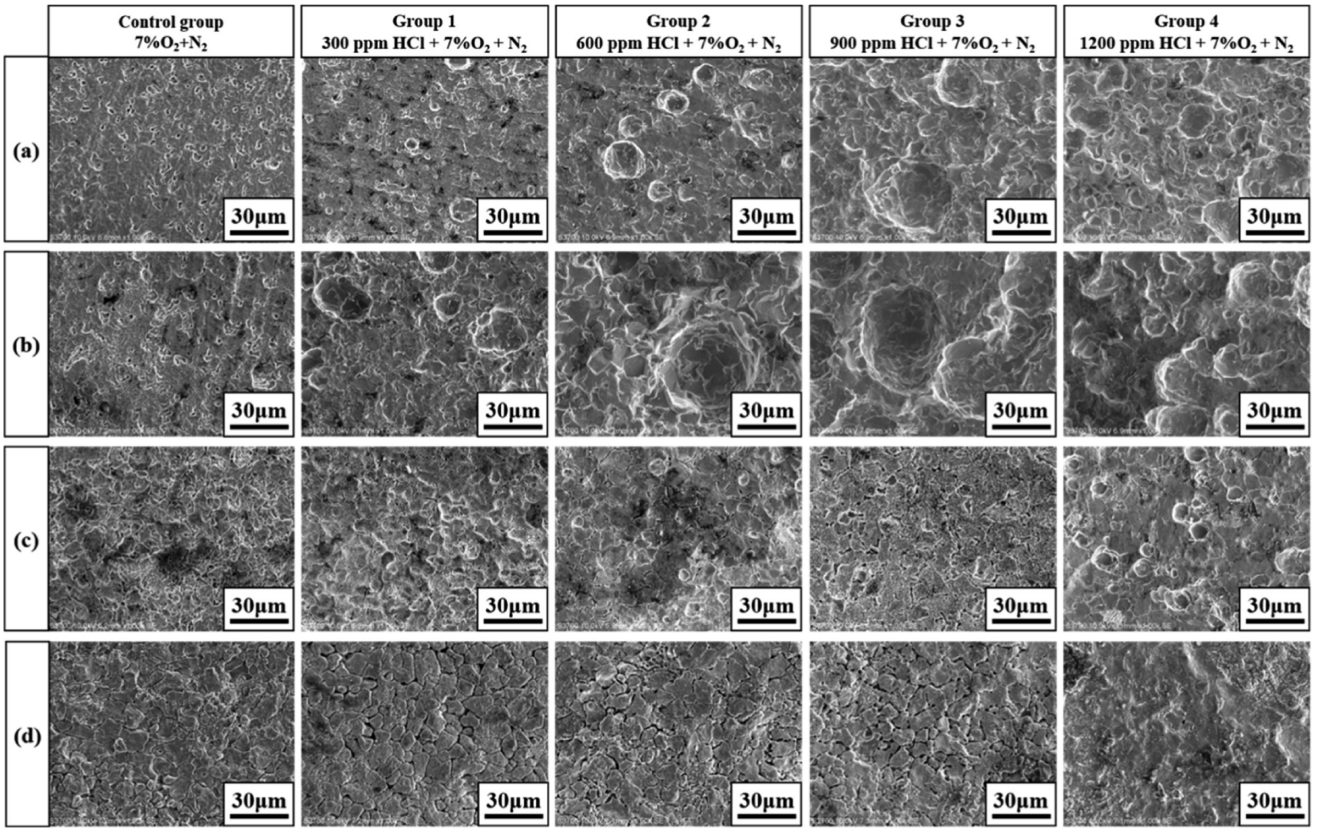

Figure 3. SEM images of the corroded surfaces of 12Cr1MoV alloy after removing corrosion products according to ISO 8407-2021; rows a, b, c, and d represent tests at 460, 510, 545, and 580 °C, respectively. Columns correspond to different concentrations of HCl (as marked in the fgure).

microscope (Sigma 300, ZEISS) at 3 keV of acceleration voltage.

2.5. Thermodynamic Analysis. In the corrosion mechanism analysis part, HSC Chemistry 9.1.1 software (Outotec) was used for thermodynamic equilibrium calculations.

3. RESULTS

3.1. Corrosion Test in HCl. *3.1.1. Corrosion Kinetics.* Weight measurement was used to determine the corrosion kinetics of 12Cr1MoV alloy, which revealed the evolution of corrosion. The test conditions are named as the control group for (7% O_2 + N_2), group 1 for (300 ppm HCl + 7%O_2 + N_2), group 2 for (600 ppm HCl + 7% O_2 + N_2), group 3 for (900 ppm HCl + 7% O_2 + N_2), and group 4 for (1200 ppm HCl + 7% O_2 + N_2). As shown in Figure 2a, at 460 °C, all mass gain curves almost overlapped in the first 72 h and bifurcated after 72 h. The corrosion rates of specimens in groups 2, 3, and 4 increased sharply after 72 h. Particularly, the higher the HCl concentration, the higher the corrosion curve rose. The maximum mass gain after 168 h was 2.70 mg/cm^2, which occurred in group 4. The mass gain curve of group 1 overlapped with that of the control group throughout, both showing a parabolic law. These results suggested that the increase in the HCl concentration could accelerate the high-temperature oxidation of 12Cr1MoV at 460 °C when the HCl concentration in the environment was higher than 300 ppm.

At 510 °C (Figure 2b), an acceleration effect of HCl on corrosion was observed under the exposure environment with 300 ppm HCl (group 1). Corrosion in group 1 started slowly and then became faster. However, a more pronounced acceleration effect appeared under environments with high concentrations of HCl. In groups 2, 3, and 4, the corrosion curves almost overlapped. Corrosion started fast and then slightly slowed down, showing a parabolic shape. The mass gains were significantly higher than those of the other two groups from the early stage of corrosion. Ultimately, the maximum mass gain of 6.76 mg/cm^2 was reached in group 2, which was 8 times that of the control group. Moreover, the maximum mass gain at 510 °C was twice as much as that at 460 °C, which indicated that the corrosion was strongly accelerated by the increase in temperature.

At 545 °C, compared with the control group without HCl, the addition of HCl had a significant effect on the corrosion rate of the specimens (Figure 2c). Although growing at the same rate as group 1 during the first 72 h, groups 2, 3, and 4 experienced a sharp increase in mass gain after 72 h, while the mass gain of group 1 always increased steadily and parabolically. The final maximum mass gain was 6.53 mg/cm^2, which is exceedingly close to that at 510 °C, indicating that the high-temperature oxychloride corrosion of the specimens was not enhanced by increasing the temperature from 510 to 545 °C.

Interestingly, at 580 °C (Figure 2d), in the control group without HCl addition, the 12Cr1MoV alloy was not oxidized more severely with the increase in temperature than at low temperatures, whose mass gain at 168 h still did not exceed 2 mg/cm^2. However, at 580 °C, an obvious severe corrosion was displayed in all test groups with HCl-added. In groups 1, 2, 3, and 4, corrosion developed in a similar trend. They all started with a linear increase and then slightly slowed down. However, at 168 h, the maximum mass gain they achieved was different. Under environments containing 300, 600, 900, and 1200 ppm HCl, the specimens reached 9.91, 12.38, 14.92, and 12.12 mg/

https://doi.org/10.1021/acsomega.2c02722
ACS Omega 2022, 7, 23929−23938

cm^2 of mass gain, respectively, after 168 h of exposure. These results showed that the detrimental effect of HCl, especially high concentrations of HCl, on specimens was more significant at 580 °C, but this effect was not further exacerbated when the concentration of HCl exceeded 900 ppm.

3.1.2. Corrosion Morphology. After corrosion products were removed, the corroded surfaces of all alloy specimens were investigated by SEM. As illustrated in Figure 3, typical morphologies of corrosion features such as pits, cracks, and grain boundaries could be identified on the corroded surfaces.

In the control group, some small pits (1−5 μm in diameter) were identifiable on the specimen surface at 460 °C, and by 510 °C, these pits tended to enlarge and interconnect. By 545 °C, these pits were fully connected, turning into a continuous network of cracks. Finally, by 580 °C, there was no new change on the surface of the specimen.

In group 1, larger pits (6−15 μm in diameter) appeared on the specimen surface at 460 °C, compared with the control group. As the temperature increased to 510 °C, the diameter of the pits increased to 15−30 μm. However, by 545 °C, these pits disappeared and were replaced by shallow cracks. Furthermore, by 580 °C, these cracks have turned into deep grain boundaries, and loose grains were visible. Similarly, in group 2, the pits with diameters of 12.5−20 μm first existed on the specimen surface at 460 °C, and then larger pits with a diameter of 50 μm appeared at 510 °C. Then, at 545 °C, shallow cracks replaced the pits, and finally, at 580 °C, the surface of the specimen was covered by festering network-like deep cracks.

In group 3, corrosion further deteriorated. The pits with diameters of 22.5∼45 μm were observed on the specimen surface at 460 °C. Then, at 510 °C, the pits with a diameter of 55 μm and cylindrical grooves with a diameter of 25 μm dominated. By 545 °C, a messy mesh of cracks spread all over the metal surface. By 580 °C, the surface of the specimen was eroded with interconnected holes, which means the metal experienced severe corrosion. Interestingly, in group 4, the size of pits at 460 and 510 °C did not increase compared with those in group 3. Moreover, cracks were not found at 545 and 580 °C, and this phenomenon is in agreement with the kinetics results that the corrosion rate decreased when the concentration of HCl increased from 900 to 1200 ppm at 545 and 580 °C (Figure 2c,d).

The SEM results in Figure 3 indicated that both the concentration of HCl and the temperature affected the corrosion of 12Cr1MoV alloy. The effect of the concentration of HCl was mainly reflected in the expansion or deepening of the corrosion pits or cracks on the surfaces of the specimens with the increase of the concentration of HCl. The influence of temperature was primarily reflected in the types of corrosion characteristics. At 460 and 510 °C, pits were formed on the surfaces of the specimens, while at 545 and 580 °C, cracks were formed, implying severe failure.

Figure 4 showed surface micromorphologies of corrosion products of 12Cr1MoV alloy in an oxidizing atmosphere containing 600 ppm HCl at different temperatures for 168 h. The specimens were fully covered by a loose, disordered, and rough grain structure at 460 and 510 °C (Figure 4a,b). With the increase in temperature, the structure transformed into a looser and porous network structure at 545 °C, accompanied by fine cracks and bulges (Figure 4c). At 580 °C, the structure became a significant crack and tended to spall (as shown in Figure 4d). These results suggested that the corrosion products

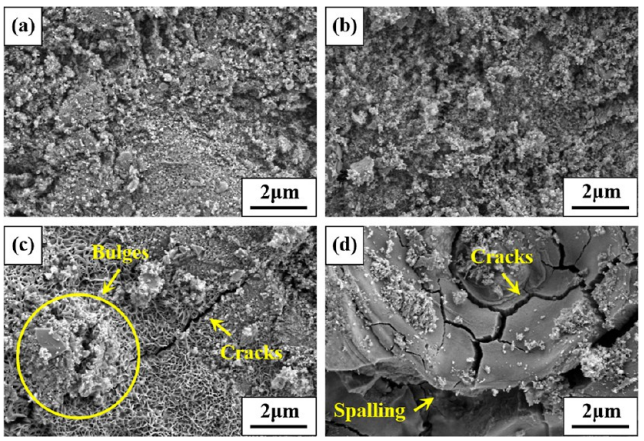

Figure 4. SEM images of the surfaces of 12Cr1MoV alloy exposed to 600 ppm HCl + 7% O_2 + N_2 for 168 h at (a) 460, (b) 510, (c) 545, and (d) 580 °C (corrosion products retained).

of 12Cr1MoV alloy were loose and porous in the presence of HCl, in particular, at 545 and 580 °C.

3.2. Corrosion Test in SO_2. *3.2.1. Corrosion Kinetics.* Weight measurement was also conducted in SO_2 series tests (Figure 5). The test conditions are named as reference condition (7% O_2 + N_2), condition 1 for (50 ppm SO_2 + 7% O_2 + N_2), condition 2 for (100 ppm SO_2 + 7% O_2 + N_2), condition 3 for (150 ppm SO_2 + 7% O_2 + N_2), and condition 4 for (200 ppm SO_2 + 7% O_2 + N_2). At 460 °C (Figure 5a), the mass gain of specimens in each condition was generally low, even the maximum mass gain at 168 h did not exceed 0.8 mg/cm^2. The mass gain curves of the conditions with added SO_2 were all parabolic, but unexpectedly the curve in the reference condition without SO_2 showed a trend of first linear increase and then a slight slowdown. As shown in Figure 5b, at 510 °C, with the increase of exposure time, the mass gain curves of each condition all exhibited a parabolic trend, but these curves almost overlapped, so the effect of SO_2 on corrosion was not reflected. Likewise, at 545 °C (Figure 5c), the curves of conditions 1, 2, 4, and the reference condition were parabolic and corrosion was not accelerated with the addition of SO_2, even was mitigated under the environment containing 200 ppm SO_2. However, one exception was that the curve of condition 3 showed a steep rise after 72 h, deviating from the parabolic trend and eventually surpassing all other curves. At 580 °C (Figure 5d), the corrosion curves of the five conditions were also parabolic and almost staggered together, showing a pattern independent of the SO_2 concentration. The above results suggested that the addition of SO_2 concentrations as low as 0−200 ppm to the oxidizing atmosphere did not lead to a deleterious effect on the 12Cr1MoV alloy at 460−580 °C.

3.2.2. Corrosion Morphology. A larger magnification was adopted in the SEM observation of the SO_2 series test (Figure 6). Unlike the severe corrosion in the HCl series test, the corroded surfaces of the specimens in oxidizing atmospheres containing SO_2 exhibited relatively minor damage. As can be seen from Figure 6, regardless of the temperature, there was no significant difference in the specimen surface between the specimen surfaces of the conditions with SO_2 and the reference condition without SO_2. This result again proves that the presence of low-concentration SO_2 in the oxidizing atmosphere cannot affect the high-temperature oxidation of 12Cr1MoV. In addition, the change brought by the increase in temperature

https://doi.org/10.1021/acsomega.2c02722
ACS Omega 2022, 7, 23929−23938

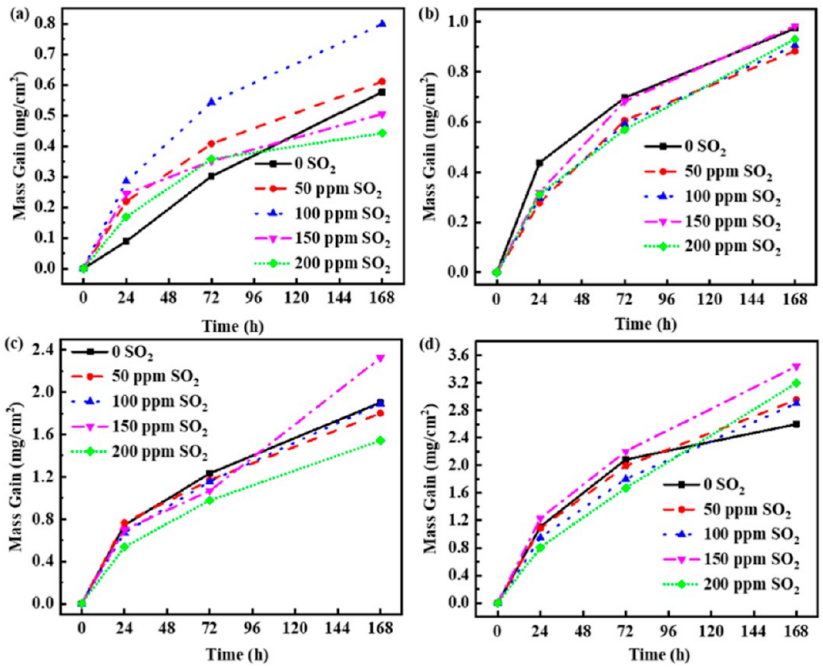

Figure 5. Mass gain of 12Cr1MoV alloy exposed to oxidizing atmosphere containing different concentrations of SO_2 at (a) 460, (b) 510, (c) 545, and (d) 580 °C for 168 h.

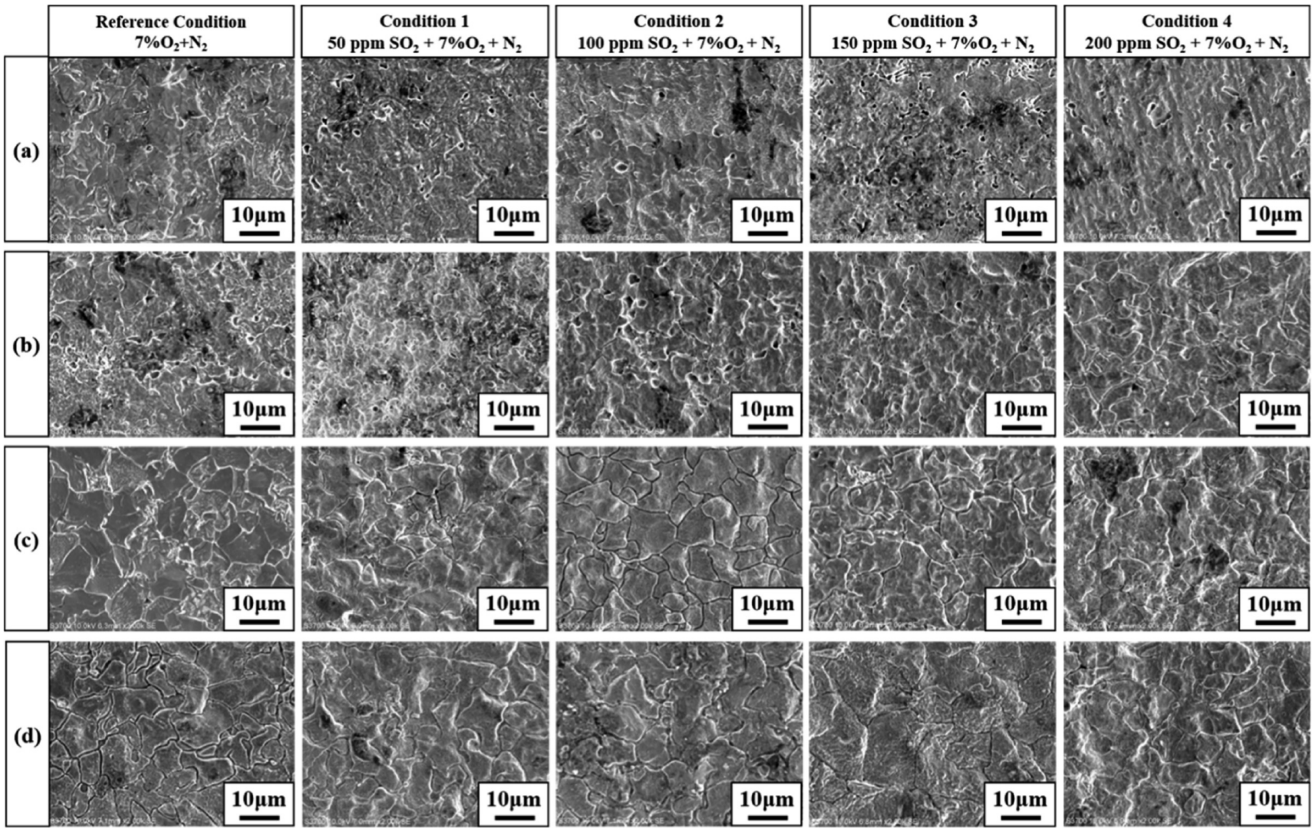

Figure 6. SEM images of the corroded surfaces of 12Cr1MoV alloy specimens after removing the corrosion products according to ISO 8407-2021; rows a, b, c, and d represent tests at 460, 510, 545, and 580 °C, respectively. Columns correspond to different concentrations of SO_2 (as marked in the figure).

was the appearance of cracks or grain boundaries, which was also observed in the SEM results of the HCl series.

Figure 7 showed SEM images of the corrosion product morphology of the 12Cr1MoV alloy exposed under an oxidizing environment containing 100 ppm SO_2 at different temperatures for 168 h. Compared to the SEM images in the HCl series test (Figure 4), the surfaces of corrosion products were smoother and denser in the SO_2 series test. This result

https://doi.org/10.1021/acsomega.2c02722
ACS Omega 2022, 7, 23929−23938

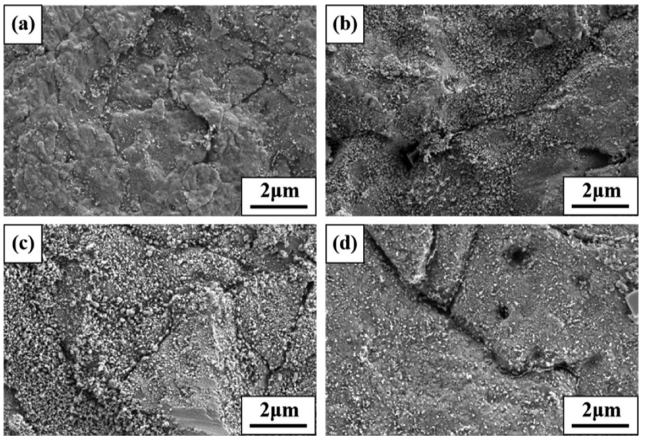

Figure 7. SEM images of the surfaces of 12Cr1MoV alloy exposed to 100 ppm SO_2 + 7% O_2 + N_2 for 168 h at (a) 460, (b) 510, (c) 545, and (d) 580 °C (corrosion products retained).

demonstrates the low corrosion rate of the 12Cr1MoV alloy in the SO_2 series test.

4. DISCUSSION

To clarify the effect of typical concentrations of corrosive media (HCl and SO_2) in MSW incineration flue gas on corrosion rates of commercial alloy commonly used in WTE superheaters, two series of corrosion tests were performed by varying the HCl concentration from 0 to 1200 ppm, and the SO_2 concentration from 0 to 200 ppm, together with simulated flue gas composition. The corrosion kinetics and corrosion morphology formed in oxidizing atmospheres containing varying HCl and SO_2 exhibited very different laws, which provided important evidence to discuss the harmfulness of typical corrosion media in MSW incineration flue gas. Therefore, there are three aspects of this problem that have to be addressed.

4.1. Comparison of Corrosivity of HCl and SO_2. The first question discussed is comparing the corrosiveness of HCl and SO_2. Regarding the reason why HCl is more harmful than SO_2, in addition to the relatively higher concentration of HCl in MSW incineration flue gas, the high activity of Cl is also a major reason for its stronger corrosiveness, in other words, once HCl is added to the oxidizing atmosphere, corrosion will be aggravated immediately. As shown in Figure 8a, in the absence of HCl, the corrosion mass gain after 168 h exposure did not exceed 2 mg/cm^2 even at 580 °C, whereas the addition of merely 300 ppm HCl resulted in a corrosion mass gain of 9.91 mg/cm^2, providing evidence of the high corrosiveness of HCl, which was also been found in an earlier investigation.[5] Remarkably, the effect of HCl was promoted by the increase in temperature, especially when the metal temperature was 580 °C, which was in agreement with the findings reported by Shang-Hsiu Lee et al.[45] Another important finding was that when the temperature was higher than 460 °C, the corrosion rate no longer increased linearly with the increase of HCl concentration but peaked at the point in which the HCl concentration was 600 or 900 ppm and then decreased. This finding implied that the effect of increasing the HCl concentration on corrosion was limited at higher temperatures. A possible explanation for this is that the oxidation film formation rate of metal is too fast at higher temperatures, which hinders the partial reaction between Cl and metal.

On the contrary, as illuminated in Figures 5 and 8b, the acceleration effect of SO_2 concentrations (0−200 ppm) on the high-temperature corrosion of 12Cr1MoV alloy was insignificant, and there may even be an inhibitory effect, which is consistent with previous studies.[29−31] The presence of trace amounts of SO_2 (0−1000 ppm) in O_2 below 600 °C has been reported to slow down the oxidation of pure iron.[29] In the present study, it was indeed observed at 460, 510, and 545 °C that when the concentration of SO_2 increased to 200 ppm, the overall mass gain decreased to a lower level than that of the reference condition. This inhibition phenomenon by sulfur was generally explained by the formation of sulfate at the gas phase and oxide interface.[29]

4.2. HCl Corrosion Kinetics and the Proposed Mechanism. The second problem is about the relation between corrosion kinetics and the HCl concentration. It is worth mentioning that the corrosion kinetics under different HCl concentrations were not always the same at four temperatures (Figure 2). For instance, in the test groups with high concentrations of HCl (600−1200 ppm), the corrosion rates suddenly increased after a 72 h incubation period at 460 and 545 °C (Figure 2a,c), while at 510 and 580 °C (Figure 2b,d), the corrosion rates under these conditions were initially high and then decreased slightly. This phenomenon may be related to the random cracking of corrosion products.

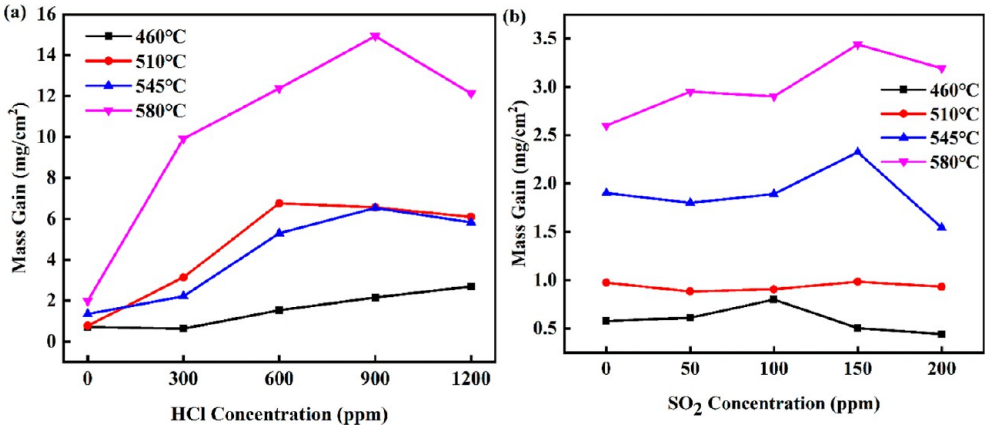

Figure 8. Overall mass gain at 168 h vs (a) HCl concentrations and (b) SO_2 concentrations for 12Cr1MoV alloy at different temperatures.

https://doi.org/10.1021/acsomega.2c02722
ACS Omega 2022, 7, 23929−23938

As shown in Figure 2a,c, it could be explained that the corrosion product cracked or fell off at 72 h because of the internal stress in corrosion product films, which led to the exposure of the fresh substrate to the ambient atmosphere. In this case, the surface of the substrate was more easily penetrated by the chlorine due to the existence of cracks or pits, resulting in a rapid increase in mass. Similarly, from Figure 2b,d, it could be explained that the corrosion products were easy enough to fall off from the beginning of the corrosion, so the corrosion mass gains increased linearly from 0 to 72 h and then slowed down slightly. However, the slight decrease in the corrosion rate from 72 to 168 h was solely a result of a comparison with the initial high-speed corrosion. Therefore, it is still high, and it cannot be assumed that the corrosion rate will decrease with time. The shedding of corrosion products is accidental and irregular, and the test operation and test parameters may affect it, but it is certain that, as is obvious in Figure 2, when the HCl concentration in the environment increases, the corrosion curve is difficult to maintain the parabolic trend, that is, corrosion products are more easily sloughed off in such a circumstance. Moreover, evidence that the corrosion rate is higher in the environment with a high concentration of HCl is that relatively larger pits and deeper cracks formed on the metal surface make the metal vulnerable to attack (as shown in Figures 3 and 4). Therefore, the use of steam soot blowing in WTE plants is likely to shorten the life of the superheater tube bundles.

In light of the results obtained, the alloy experienced pitting corrosion at 460−545 °C and severe failure at 580 °C. It is important to analyze the possible corrosion mechanism of the 12Cr1MoV alloy in HCl + O_2 + N_2 at high temperatures. According to the calculation results of the thermodynamic software, the formation of Cl_2 and H_2O through reaction 3 is thermodynamically favored. Therefore, the main aggressive species in corrosion may be Cl_2, O_2, and H_2O, not HCl and O_2.

$$4HCl(g) + O_2(g) = 2Cl_2(g) + 2H_2O(g) \quad (3)$$

When these species come into contact with Fe at high temperatures, the following reactions may occur

$$4Fe + 3O_2(g) = 2Fe_2O_3 \quad (4)$$

$$3Fe + 4H_2O(g) = Fe_3O_4 + 4H_2(g) \quad (5)$$

$$2Fe + 3H_2O(g) + 1.5O_2(g) = 2Fe(OH)_3 \quad (6)$$

$$2Fe(OH)_3 = Fe_2O_3 + 3H_2O(g) \quad (7)$$

Thus, during oxide formation, gases including H_2 and H_2O generated by reactions 5 and 7 will lead to a porous oxide layer, providing a channel for the inward diffusion of corrosive gases. Then, Cl_2 will easily enter the scale−metal interface through the cracks or pores in the oxide layer and react with the metal substrate

$$2Fe + 3Cl_2(g) = 2FeCl_3(g) \quad (8)$$

$$Fe + Cl_2(g) = FeCl_2(s) \quad (9)$$

$$3FeCl_3 + 2O_2(g) = Fe_3O_4 + 4.5Cl_2(g) \quad (10)$$

$$3FeCl_2 + 2O_2(g) = Fe_3O_4 + 3Cl_2(g) \quad (11)$$

In reactions 10 and 11, if Fe_3O_4 is replaced by Fe_2O_3, these reactions are also thermodynamically spontaneous. The presence of Cl_2 reacted with Fe, forming metal chlorides according to reactions 8−11. Therefore, "active oxidation" occurs. The Cl_2 produced in reactions 10 and 11 will continue to participate in the next attack (reactions 8 and 9), acting as a catalyst to accelerate corrosion.

It is the incomplete contact of Cl_2 with the substrate, entering the scale−metal interface through the cracks or pores in the oxide layer, that lead to the formation of pitting pits (Figure 3). As the loose oxide accumulates more and more, the internal stress within the oxide increases, and bulging and spalling (Figure 4c,d) are prone to occur, especially at high temperatures. Once the oxide is exfoliated, the substrate will be exposed, and then the corrosion will be accelerated again (as shown in Figure 2).

4.3. SO_2 Corrosion Kinetics and Proposed Mechanism. The third aspect deals with the corrosion rates in the SO_2 series of tests. As presented in Figure 5, the kinetic curves in the SO_2 series of tests all showed a parabolic trend, indicating that the corrosion products formed under these conditions had protective effects and could retard the further attack of external gas. In other words, the diffusion through the growing corrosion products is the limiting process of the corrosion process.[46] For a parabolic corrosion mass gain curve, the square of the mass gain per unit surface area of the specimen is linearly related to the exposure time, so its slope k_p can be further used to study the corrosion rates of the specimens. As clarified in Figure 9, the change in the SO_2 concentration has little effect on the corrosion rate. On the contrary, regardless of the SO_2 concentration in the atmosphere, the k_p value increased obviously with the increase of temperature, in particular at 545 and 580 °C increased dramatically, demonstrating a strong temperature dependence of corrosion. Besides, compared to the SEM results of the HCl series, it can be seen from the microscopic morphology (seeing Figure 6) that in the presence of SO_2, the pitting pits formed on the surface of the sample were only 2−3 μm, and no cracks were formed at any temperature, and the surfaces of the substrates were relatively smoother, which also proved the low corrosion rate in this case.

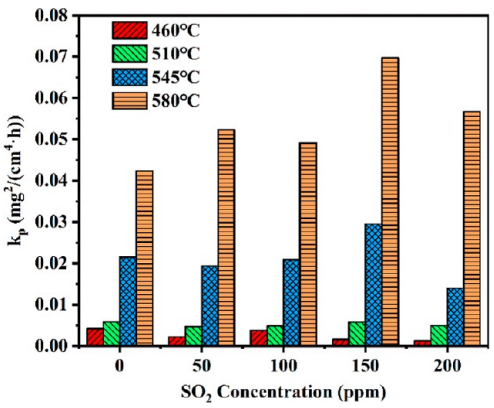

Figure 9. Parabolic rate constants for the SO_2 series corrosion test.

Under the condition of SO_2 + O_2 + N_2, there is no H element in the system, so H_2O will not be generated. In other words, corrosion develops under completely high temperature and dry conditions. From a thermodynamic point of view, only metal oxidation and sulfation reactions (reactions 4 and 12) can occur practically.

https://doi.org/10.1021/acsomega.2c02722
ACS Omega 2022, 7, 23929−23938

$$3SO_2(g) + 2Fe + 3O_2(g) = Fe_2(SO_4)_3 \quad (12)$$

In a previous investigation, it is hypothesized that the sulfate formed on the metal surface blocked the surface sites where oxide ions are generated, thereby slowing down the oxidation rate of Fe.[29] Although this inhibitive effect of traces of SO_2 on the oxidation behavior of 12Cr1MoV alloy was also demonstrated in this study, this hypothesis could not be effectively verified and still needed further exploration.

5. CONCLUSIONS

In conclusion, the results of this study demonstrated that the addition of 300−1200 ppm HCl to the oxidizing atmosphere increased the corrosion rate of 12Cr1MoV at all four test temperatures, but the relation between the HCl concentration and the corrosion rate was not always linear. On the other hand, we also confirmed that the low concentration of SO_2 in the oxidizing gas did not cause accelerated corrosion but may inhibit corrosion. Furthermore, both series of test results consistently proved that the temperature had a pronounced influence on the corrosion of 12Cr1MoV alloy, in particular, at 580 °C. Collectively, our data demonstrate that the addition of HCl is more corrosive than that of SO_2 under an oxidizing atmosphere, and the effect of temperature on corrosion is significant.

AUTHOR INFORMATION

Corresponding Author

Xuguang Jiang − *State Key Laboratory of Clean Energy Utilization, Institute for Thermal Power Engineering, Zhejiang University, Hangzhou 310027 Zhejiang, China; Zhejiang University Qingshanhu Energy Research Center, 311305 Hangzhou, P. R. China;* orcid.org/0000-0002-8543-1613; Email: jiangxg@zju.edu.cn

Authors

Xiaobo Liu − *State Key Laboratory of Clean Energy Utilization, Institute for Thermal Power Engineering, Zhejiang University, Hangzhou 310027 Zhejiang, China; Zhejiang University Qingshanhu Energy Research Center, 311305 Hangzhou, P. R. China*

Yin Duan − *State Key Laboratory of Clean Energy Utilization, Institute for Thermal Power Engineering, Zhejiang University, Hangzhou 310027 Zhejiang, China; Zhejiang University Qingshanhu Energy Research Center, 311305 Hangzhou, P. R. China*

Qian Chen − *State Key Laboratory of Clean Energy Utilization, Institute for Thermal Power Engineering, Zhejiang University, Hangzhou 310027 Zhejiang, China; Zhejiang University Qingshanhu Energy Research Center, 311305 Hangzhou, P. R. China*

Ling Long − *State Key Laboratory of Clean Energy Utilization, Institute for Thermal Power Engineering, Zhejiang University, Hangzhou 310027 Zhejiang, China; Zhejiang University Qingshanhu Energy Research Center, 311305 Hangzhou, P. R. China*

Guojun Lv − *State Key Laboratory of Clean Energy Utilization, Institute for Thermal Power Engineering, Zhejiang University, Hangzhou 310027 Zhejiang, China; Zhejiang University Qingshanhu Energy Research Center, 311305 Hangzhou, P. R. China*

Qunxing Huang − *State Key Laboratory of Clean Energy Utilization, Institute for Thermal Power Engineering, Zhejiang University, Hangzhou 310027 Zhejiang, China; Zhejiang University Qingshanhu Energy Research Center, 311305 Hangzhou, P. R. China;* orcid.org/0000-0003-1557-3955

Complete contact information is available at: https://pubs.acs.org/10.1021/acsomega.2c02722

Author Contributions

X.J. and Q.H. contributed to the conception and design of the study. G.L. and L.L. organized the database. Y.D. and Q.C. performed the statistical analysis. X.L. wrote the first draft of the manuscript. All authors contributed to manuscript revision and read and approved the submitted versions.

Funding

This study was supported by the National Key Research and Development Program of China [grant no 2018YFC1901302] and the Innovative Research Groups of the National Natural Science Foundation of China [grant no. 51621005].

Notes

The authors declare no competing financial interest.

REFERENCES

(1) Brunner, P. H.; Rechberger, H. Waste to energy-key element for sustainable waste management. *Waste Manage.* **2015**, *37*, 3−12.

(2) Wienchol, P.; Szlęk, A.; Ditaranto, M. Waste-to-energy technology integrated with carbon capture-challenges and opportunities. *Energy* **2020**, *198*, 117352.

(3) Zhang, D.; Huang, G.; Xu, Y.; Gong, Q. Waste-to-Energy in China: Key challenges and opportunities. *Energies* **2015**, *8*, 14182−14196.

(4) National Bureau of Statistics of China. *China Statistical Yearbook*; China Statistics Press: Beijing, 2020.

(5) Jonsson, T.; Folkeson, N.; Halvarsson, M.; Svensson, J.-E.; Johansson, L.-G. Microstructural investigation of the HCl-induced corrosion of the austenitic alloy 310S (52Fe26Cr19Ni) at 500°C. *Oxid. Met.* **2014**, *81*, 575−596.

(6) Wenga, T.; Chen, G.; Ma, W.; Yan, B. Study on corrosion kinetics of 310H in different simulated MSW combustion environment. The influence of SO_2 and H_2O on NaCl assisted corrosion. *Corros. Sci.* **2019**, *154*, 254−267.

(7) Viklund, P.; Hjörnhede, A.; Henderson, P.; Stålenheim, A.; Pettersson, R. Corrosion of superheater materials in a waste-to-energy plant. *Fuel Process. Technol.* **2013**, *105*, 106−112.

(8) Schaal, E.; David, N.; Panteix, P. J.; Rapin, C.; Brossard, J. M.; Maad, F. Effect of chloride content in ash in oxidation kinetics of Ni-Based and Fe-Based alloys. *Oxid. Met.* **2015**, *84*, 307−327.

(9) Asteman, H.; Spiegel, M. Investigation of the HCl (g) attack on pre-oxidized pure Fe, Cr, Ni and commercial 304 steel at 400°C. *Corros. Sci.* **2007**, *49*, 3626−3637.

(10) Zahs, A.; Spiegel, M.; Grabke, H. J. Chloridation and oxidation of iron, chromium, nickel and their alloys in chloridizing and oxidizing atmospheres at 400-700°C. *Corros. Sci.* **2000**, *42*, 1093−1122.

(11) Grabke, H. J.; Reese, E.; Spiegel, M. The effects of chlorides, hydrogen chloride, and sulfur dioxide in the oxidation of steels below deposits. *Corros. Sci.* **1995**, *37*, 1023−1043.

(12) Folkeson, N.; Johansson, L.-G.; Svensson, J.-E. Initial stages of the HCl-induced high-temperature corrosion of alloy 310. *J. Electrochem. Soc.* **2007**, *154*, C515.

(13) Sadeghimeresht, E.; Reddy, L.; Hussain, T.; Huhtakangas, M.; Markocsan, N.; Joshi, S. Influence of KCl and HCl on high temperature corrosion of HVAF-sprayed NiCrAlY and NiCrMo coatings. *Mater. Des.* **2018**, *148*, 17−29.

(14) Bramhoff, D.; Grabke, H. J.; Reese, E.; Schmidt, H. P. Influence of HCl and Cl_2 on high temperature corrosion of 2 1/4 Cr1Mo steel in atmospheres with high oxygen pressures. *Werkst. Korros.* **1990**, *41*, 303−307.

https://doi.org/10.1021/acsomega.2c02722
ACS Omega 2022, 7, 23929−23938

(15) Haanappel, V. A. C.; Fransen, T.; Gellings, P. J. Chlorine-induced high temperature corrosion: II. The Tedmon equation as a theoretical approach of the kinetics as a theoretical approach of the kinetics. *High Temp. Mater. Processes* **1992**, *10*, 91−100.
(16) Sharobem, T.; Castaldi, M. J. The ffect of SO2/HCl ratio on superheater high temperature corrosion. *20th Annual North American Waste-to-Energy Conference*; American Society of Mechanical Engineers (ASME): Portland, ME, United states, 2012, pp 23-27.
(17) Nielsen, H. P.; Frandsen, F. J.; Dam-Johansen, K.; Baxter, L. L. The implications of chlorine-associated corrosion on the operation of biomass-fired boilers. *Prog. Energy Combust.* **2000**, *26*, 283−298.
(18) Żurek, Z.; Gilewicz-Wolter, J.; Hetmańczyk, M.; Dudała, J.; Stawiarski, A. High temperature corrosion of chromium-manganese steels in sulfur dioxide. *Oxid. Met.* **2005**, *64*, 379−395.
(19) Xu, H.; Zhou, S.; Zhu, Y.; Xu, W.; Xiong, X.; Tan, H. Experimental study on the effect of H_2S and SO_2 on high temperature corrosion of 12Cr1MoV. *Chin. J. Chem. Eng.* **2019**, *27*, 1956−1964.
(20) Falk, F.; Menneken, M.; Stephan-Scherb, C. Real-time observation of high-temperature gas corrosion in dry and wet SO_2-containing atmosphere. *JOM* **2019**, *71*, 1560−1565.
(21) Okoro, S. C.; Montgomery, M.; Frandsen, F. J.; Pantleon, K. High temperature corrosion under laboratory conditions simulating biomass-firing: a comprehensive characterization of corrosion products. *Energy Fuels* **2014**, *28*, 6447−6458.
(22) Gilewicz-Wolter, J.; Żurek, Z. Corrosion of iron in sulfur dioxide at 0.1 MPa. *Oxid. Met.* **1996**, *45*, 469.
(23) Gillot, B.; Radid, M. Corrosion in SO_2 of chromium and manganese at high temperature. *Oxid. Met.* **1990**, *33*, 279−299.
(24) Gesmundo, F.; de Asmundis, C.; Merlo, S.; Bottino, C. The corrosion of iron in pure SO_2 under different pressures at 700°C. *Mater. Corros.* **1979**, *30*, 179.
(25) Nützmann, K.; Kranzmann, A.; Stephan-Scherb, C. The influence of chromium on early high temperature corrosion of ferritic alloys under SO_2 atmosphere. *Mater. High-Temp.* **2018**, *35*, 558−568.
(26) Yu, C.; Zhang, J.; Young, D. J. High temperature corrosion of Fe-Cr-(Mn/Si) alloys in CO_2-H_2O-SO_2 gases. *Corros. Sci.* **2016**, *112*, 214−225.
(27) Rahmel, A. Kinetic conditions for the simultaneous formation of oxide and sulphide in reactions of iron with gases containing sulphur and oxygen or their compounds. *Corros. Sci.* **1973**, *13*, 125−136.
(28) Haflan, B.; Kofstad, P. The reaction of nickel with SO_2 + O_2/SO_3 at 500-900°C. *Corros. Sci.* **1983**, *23*, 1333−1352.
(29) Järdnäs, A.; Svensson, J. E.; Johansson, L. G. The inhibitive effect of traces of SO_2 on the oxidation of iron. *Oxid. Met.* **2003**, *60*, 427−445.
(30) Jonsson, T.; Järdnäs, A.; Svensson, J.-E.; Johansson, L.-G.; Halvarsson, M. The effect of traces of SO_2 on iron oxidation: A microstructural study. *Oxid. Met.* **2007**, *67*, 193−213.
(31) Järdnäs, A.; Svensson, J.; Johansson, L. Influence of SO_2 on the oxidation of 304L steel in O_2 + 40%H_2O at 600°C. *Oxid. Met.* **2008**, *69*, 249−263.
(32) Lee, H.; Yi, S.-M.; Holsen, T. M.; Seo, Y.-S.; Choi, E. Estimation of CO_2 emissions from waste incinerators: comparison of three methods. *Waste Manage.* **2018**, *73*, 247−255.
(33) Bal, M.; Siddiqi, H.; Mukherjee, S.; Meikap, B. C. Design of self priming venturi scrubber for the simultaneous abatement of HCl gas and particulate matter from the flue gas. *Chem. Eng. Res. Des.* **2019**, *150*, 311−319.
(34) Dal Pozzo, A.; Lazazzara, L.; Antonioni, G.; Cozzani, V. Techno-economic performance of HCl and SO_2 removal in waste-to-energy plants by furnace direct sorbent injection. *J. Hazard. Mater.* **2020**, *394*, 122518.
(35) Dal Pozzo, A.; Guglielmi, D.; Antonioni, G.; Tugnoli, A. Environmental and economic performance assessment of alternative acid gas removal technologies for waste-to-energy plants. *Sustain. Prod. Consum.* **2018**, *16*, 202−215.
(36) Zhang, H.; Yu, S.; Shao, L.; He, P. Estimating source strengths of HCl and SO_2 emissions in the flue gas from waste incineration. *J. Environ. Sci.* **2019**, *75*, 370−377.
(37) Sánchez Pastén, M.; Spiegel, M. High temperature corrosion of metallic materials in simulated waste incineration environments at 300-600°C. *Mater. Corros.* **2006**, *57*, 192−195.
(38) Li, Y. S.; Niu, Y.; Spiegel, M. High temperature interaction of Al/Si-modified Fe-Cr alloys with KCl. *Corros. Sci.* **2007**, *49*, 1799−1815.
(39) Pan, T. J.; Gesmundo, F.; Niu, Y. Corrosion behavior of three iron-based model alloys in reducing atmospheres containing HCl and H_2S at 600°C. *Corros. Sci.* **2007**, *49*, 1362−1377.
(40) Abels, J.-M.; Strehblow, H.-H. A surface analytical approach to the high temperature chlorination behaviour of inconel 600 at 700°C. *Corros. Sci.* **1997**, *39*, 115−132.
(41) He, J.; Bao, J.; Long, K.; Li, C.; Wang, G. Study on the corrosion fatigue properties of 12Cr1MoV steel at high temperature in different salt environments. *Metals* **2019**, *9*, 774.
(42) Andersson, S.; Blomqvist, E. W.; Bäfver, L.; Jones, F.; Davidsson, K.; Froitzheim, J.; Karlsson, M.; Larsson, E.; Liske, J. Sulfur recirculation for increased electricity production in waste-to-Energy plants. *Waste Manage.* **2014**, *34*, 67−78.
(43) Bai, M.; Reddy, L.; Hussain, T. Experimental and thermodynamic investigations on the chlorine-induced corrosion of HVOF thermal sprayed NiAl coatings and 304 stainless steels at 700°C. *Corros. Sci.* **2018**, *135*, 147−157.
(44) Sadeghimeresht, E.; Reddy, L.; Hussain, T.; Markocsan, N.; Joshi, S. Chlorine-induced high temperature corrosion of HVAF-sprayed Ni-based alumina and chromia forming coatings. *Corros. Sci.* **2018**, *132*, 170−184.
(45) Shang-Hsiu Lee, M. J. C. The effects of varied hydrogen chloride gas concentrations on corrosion rates of commercial tube alloys under simulated environment of WTE facilities. In *16th Annual North American Waste-to-Energy Conference*: Philadelphia, Pennsylvania, USA, 2008.
(46) Mlonka-Mędrala, A.; Magdziarz, A.; Kalemba-Rec, I.; Nowak, W. The influence of potassium-rich biomass ashes on steel corrosion above 550°C. *Energy Convers. Manage.* **2019**, *187*, 15−28.

https://doi.org/10.1021/acsomega.2c02722
ACS Omega 2022, 7, 23929−23938